

EXTENSION OF LYSAK APPROACH TO EVALUATE THE WALL PRESSURE SPECTRUM FOR BOUNDARY LAYER FLOWS

Bertrand Aupoix

ONERA, The French Aerospace Lab
F-31055, Toulouse, France
Bertrand.Aupoix@onera.fr

ABSTRACT

An analytical model proposed by Lysak to evaluate the wall pressure fluctuation spectrum and variance for pipe flows was extended to use it as a post-processor of RANS computations, whatever the turbulence model.

The model fairly reproduces key features of the wall pressure spectrum such as the f^2 behaviour in the low frequency range, the inertial f^{-1} region and the viscous cut-off. The model allows identifying the contribution of each part of the boundary layer to the wall pressure spectrum.

The model was validated for zero pressure gradient boundary layer flows. For adverse pressure gradient boundary layers, departures from experiments are observed and several plausible causes are pointed out.

INTRODUCTION

Aero-acoustics applications as well as fluid/structure coupling require information about the wall pressure spectrum. Such data are not directly provided by RANS computations which remain nowadays the industry workhorse but require turbulence resolving approaches which are much more expensive. However, models were proposed to derive the wall pressure spectrum from averaged quantities. Recently, Lysak (2006) proposed such a model for pipe flows. The present work addresses the extension of Lysak model to use it to post-process RANS computations.

LYSAK MODEL

Lysak model for the wall pressure variance is based upon classical arguments which will be shortly reminded and discussed below. The reader should refer to Lysak (2006) for more information.

- The Poisson equation is deduced from the Navier–Stokes equations. For incompressible flows, it relates the pressure at a given point to the velocity field in the whole domain. Following Kraichnan’s proposal (1956) (see Willmarth (1975)), Lysak only retains the linear term linked to the mean velocity gradient, although the turbulence/turbulence term, or non-linear term, in the Poisson equation has been shown to affect the low frequency part of the spectrum (Lee *et al.*, 2005).

- Assuming that the wall normal pressure gradient is null at the wall allows to get rid of the surface integrals in the Green operator used to solve the Poisson equation, so that the wall pressure is expressed with the help of only one volume integral.

- Assuming homogeneity in planes parallel to the wall, this volume integral reduces to an integral along the wall normal.

- The problem is translated to the Fourier space and is strongly simplified assuming that the two point velocity correlation is symmetric, a doubtful assumption for wall turbulence.

- Taylor’s hypothesis is used to assume that turbulence is frozen and convected at the local average speed. A von Kármán spectrum is used to represent the turbulent field. Such a spectrum fairly describes isotropic turbulence but its use is much more questionable for wall turbulence.

The final model reads

$$\Phi_{pp}(\omega) \approx 3\rho^2 \int_0^\infty \left(\frac{\partial U}{\partial y} \right)^2 \frac{\langle v'^2 \rangle \omega^2}{U^3 \kappa_e^4} I \left(\frac{\omega}{U \kappa_e}, \kappa_e y \right) dy$$

$$\text{where } I(\xi, \alpha) = \int_{-\infty}^\infty \frac{\exp[-2\alpha\sqrt{\xi^2 + \zeta^2}]}{(1 + \xi^2 + \zeta^2)^{17/6}} d\zeta \quad (1)$$

where Φ_{pp} is the wall pressure spectrum, ω the frequency.

The model only requires the knowledge of the mean velocity U and its gradient along the wall normal $\frac{\partial U}{\partial y}$ while the turbulent motion is described by the diagonal stress along the wall normal direction $\langle v'^2 \rangle$ and a characteristic wave number κ_e in the von Kármán spectrum.

The integration of the spectrum Φ_{pp} with respect to the frequency ω provides the wall pressure variance $\langle p'^2 \rangle$.

MODEL EXTENSIONS

Extension to three-dimensional flows

Lysak developed his model for two-dimensional pipe flows. The model is really interesting for practical applications only if it can be applied to any three-dimensional wall flow. The derivation for three-dimensional flows is similar to the original one and lengthy, so that it will not be reproduced here. Denoting U and W the velocity vector component in a plane parallel to the wall, the final model reads

$$\Phi_{pp}(\omega) \approx 3\rho^2 \int_0^\infty \left(\frac{\partial U}{\partial y} \right)^2 \frac{\langle v'^2 \rangle \omega^2}{U^3 \kappa_e^4} I \left(\frac{\omega}{U \kappa_e}, \kappa_e y, \frac{W}{U} \right) dy +$$

$$3\rho^2 \int_0^\infty \left(\frac{\partial W}{\partial y} \right)^2 \frac{\langle v'^2 \rangle U}{\kappa_e^2} J \left(\frac{\omega}{U \kappa_e}, \kappa_e y, \frac{W}{U} \right) dy$$

Coupling with turbulence models

Lysak used simple representations for the turbulent motion in pipe flows and so analytically prescribed the Reynolds stress $\langle v'^2 \rangle$ and wavenumber κ_e distributions. These data have here to be derived from information available in a RANS computation.

The analysis of DNS of two-dimensional zero pressure gradient (Spalart, 1988) and adverse pressure gradient (Skote & Henningson, 2002) boundary layers as well as pipe flows (Jimnez & Hoyas, 2008) showed that, for two-dimensional flows, the Reynolds stress $\langle v'^2 \rangle$ is better correlated with the turbulent shear $-\langle u'v' \rangle$ than with the turbulent kinetic energy k . The model used hereafter reads

$$\langle v'^2 \rangle = C_{v2}(-\langle u'v' \rangle) \quad C_{v2} = 1.3 \quad (2)$$

which fairly reproduces data, except very close to the wall where $\langle v'^2 \rangle \propto y^4$ while $-\langle u'v' \rangle \approx y^3$ so that C_{v2} should drop down to zero. No ad-hoc treatment was introduced to cope with the decrease of $\langle v'^2 \rangle$ close to the wall.

Following Lysak, the characteristic wavenumber is related to the turbulent kinetic energy k and its dissipation rate ε through the relation

$$\kappa_e = C_k \frac{\varepsilon}{k^{3/2}} \quad C_k = 1.9 \quad (3)$$

Assuming a simplified spectrum shape, with two power laws

$$E(\kappa) = \begin{cases} A\kappa^s & \text{if } \kappa \leq \kappa_e \\ K_0\varepsilon^{2/3}\kappa^{-5/3} & \text{if } \kappa \geq \kappa_e \end{cases} \quad (4)$$

the characteristic wavenumber κ_e reads

$$\kappa_e = \left(\frac{3s+5}{2(s+1)} K_0 \right)^{2/3} \frac{\varepsilon}{k^{3/2}} \quad (5)$$

von Kármán spectrum corresponds to an infrared exponent $s = 4$. With $K_0 \approx 1.4$, the above formula yields $C_k \approx 1.78$. As $1 \leq s \leq 4$, thus $1.78 \leq C_k \leq 2$ so that the value proposed by Lysak is fair.

Numerical implementation

Equation (1) requires a double integration and is rather complicate to compute accurately. Monte-Carlo method is often used, which is rather time consuming. The use of von Kármán's spectrum leads to the peculiar form of the I integral which can be used to simplify computations. Setting $Y = 2\alpha\sqrt{\xi^2 + \zeta^2} - 2\alpha\xi$, this integral reads

$$I(\xi, \alpha) = \frac{\exp(-2\alpha\xi)}{\alpha} \int_0^\infty \frac{\exp(-Y)}{\left[1 + \left(\frac{Y+2\alpha\xi}{2\alpha} \right)^2 \right]^{17/6}} \frac{Y+2\alpha\xi}{\sqrt{Y^2+4\alpha Y\xi}} dY \quad (6)$$

which can easily be evaluated using Gauss-Laguerre formula

$$\int_0^\infty \exp(-x)f(x)dx \approx \sum_{i=1}^{i=n} A_i f(x_i) \quad (7)$$

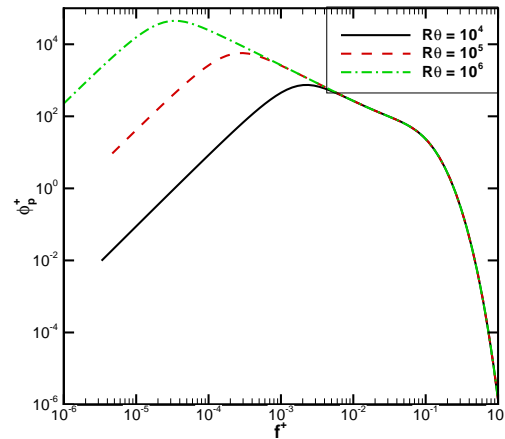


Figure 1. Non dimensional spectra using wall scaling

It was checked that a set of twelve points x_i was enough to achieve an excellent accuracy in all situations.

APPLICATION TO ZERO PRESSURE GRADIENT BOUNDARY LAYERS

Introduction

All wall pressure computations presented below rely upon boundary layer computations performed using the ONERA boundary layer software CLICET (Aupoix, 2010). This code has a self adaptive grid and it was checked that the results were insensitive to the selected grid option (standard or fine). Spectra computations were performed using four points per octave but it turned out that the same accuracy could be achieved with only one point per octave!

Results obtained using the Launder & Sharma (1974) $k - \varepsilon$ model are first discussed. Extension to other turbulence models is addressed afterwards.

Spectrum predictions

Zero pressure gradient boundary layers have been computed for Reynolds numbers based upon the momentum thickness $R\theta = 10^4, 10^5$ and 10^6 . Spectra obtained from the boundary layer profiles are plotted in figure 1. The spectra $\Phi_p(f) = 4\pi\Phi_{pp}(\omega)$ are plotted w.r.t. the frequency $f = \frac{2\pi}{\omega}$ in figure 1, using wall scaling. Scaling based upon the external velocity and the boundary layer thickness or the displacement thickness tend to collapse the low frequency part of the spectrum, but not perfectly. As expected, the higher the Reynolds number, the thicker the boundary layer and the lower the most energetic frequencies. As expected, a f^2 behaviour is obtained in the low frequency range (Bradshaw *et al.*, 1967; Farabee & Casarella, 1991) together with a f^{-1} inertial range (Bradshaw *et al.*, 1967; Panton & Linebarger, 1974). The viscous region falls steeper than the often proposed f^{-5} law. The predicted inertial range can be approximated by

$$\Phi_p^+ = \frac{2.6}{f^+} \quad \Phi_p^+ = \frac{\Phi_p}{\mu\tau_w} \quad f^+ = \frac{f\mu}{\tau_w} \quad (8)$$

the coefficient 2.6 being in the range of experimental data.

Predictions have first been validated w.r.t. experimental spectra. A nice agreement with Gravante *et al.* (1998)

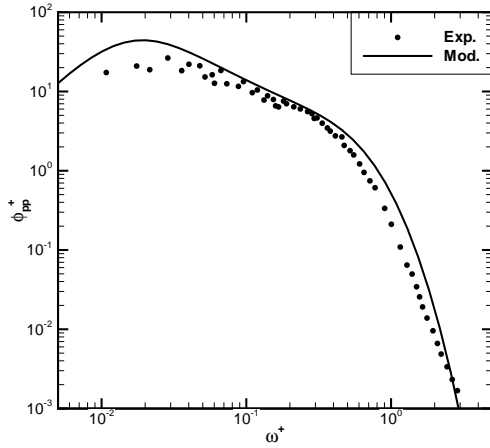


Figure 2. Wall pressure fluctuation spectra –Gravante et al. experiment

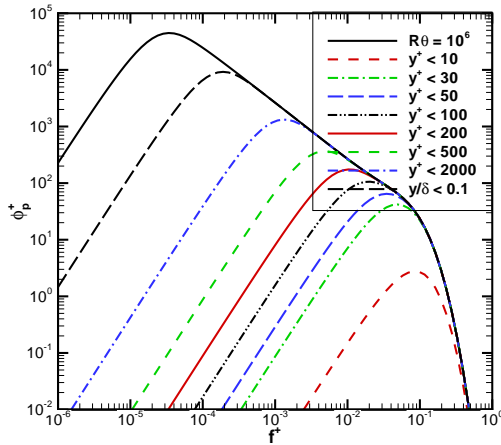


Figure 3. Contributions of the various parts of the boundary layer to the wall pressure spectrum

experiment, for $R\theta = 7076$ is shown in figure 2. It must be mentioned that the Farabee & Casarella (1991) experiment was also computed and evidenced significant differences in the low frequency part of the spectrum, which may be linked to free-stream turbulence.

Lysak (2006) points out that contributions to the wall pressure fluctuations are mainly due to the wall turbulence thanks to the $\exp(-2\kappa y)$ term while Farabee & Casarella (1991) identify contributions from all regions of the boundary layer. Figure 3 provides an analysis of the contributions of the various regions in the boundary layer, for $R\theta = 10^6$. Each “spectrum” plotted in this figure corresponds to an integration from the wall up to a given altitude. This figure clearly shows that

- the high frequency, viscous cut-off of the spectrum is the contribution of the viscous and buffer regions ($y^+ \leq 50$),
- the logarithmic region provides the inertial (f^{-1}) part of the spectrum,
- the wake region corresponds to the departure from the inertial spectrum and to the low frequency range,
- whatever the integration altitude, the low frequency part of the “spectrum” exhibits a f^2 behaviour.

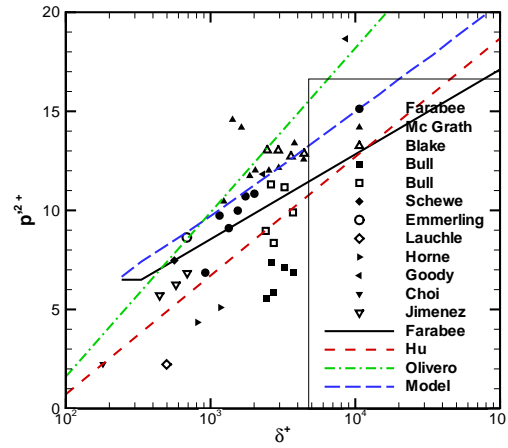


Figure 4. Evolution of the wall pressure variance the boundary layer thickness

The present result supports Lysak’s analysis but does not fully contradict Farabee & Casarella (1991) one. It must be reminded that turbulence models do not account for the inactive motions, the signature of which appears in the wall pressure. Moreover, Farabee & Casarella (1991) identified the outer layer intermittency as a source of wall pressure fluctuations, and this phenomenon is not accounted for too.

Wall pressure variance predictions

The wall pressure variance can be obtained from the integral of the spectrum as

$$\langle p^2 \rangle = \int_0^\infty \Phi_p(f) df \quad \text{or} \quad \langle p^2 \rangle^+ = \int_0^\infty \Phi_p^+(f) df^+ \quad (9)$$

The above analysis of the contributions of the various parts of the boundary layer shows that this integral can be split into three parts: the low frequency part linked to the wake contribution, the inertial range linked to the logarithmic region and the viscous part. Therefore, for a high Reynolds number, zero pressure gradient boundary layer, the viscous and low frequency contributions are constant, so that the wall pressure variance can be approximated as

$$\langle p^2 \rangle^+ = A + B \ln \delta^+ \quad (10)$$

The evolution of the pressure variance is plotted versus the boundary layer thickness in figure 4, using wall scaling. Several experimental data are plotted, the difference in the two data sets by Bull showing the strong influence of the sensor. The Farabee & Casarella (1991) correlation

$$\langle p^2 \rangle^+ = \begin{cases} 6,5 & \delta^+ \leq 333 \\ 6,5 + 1,86 \log \frac{\delta^+}{333} & \delta^+ > 333 \end{cases} \quad \delta^+ = \frac{\delta u_\tau}{\nu} \quad (11)$$

which could be considered as a reference, is also plotted as well as two other correlations from Hu *et al.* (2006) and Olivero (cited by Goody (2002)). The present model predictions are within the experimental scatter and can be fitted by the following relation

$$\langle p^2 \rangle^+ = -6.4 + 2.3 \ln \delta^+ \quad (12)$$

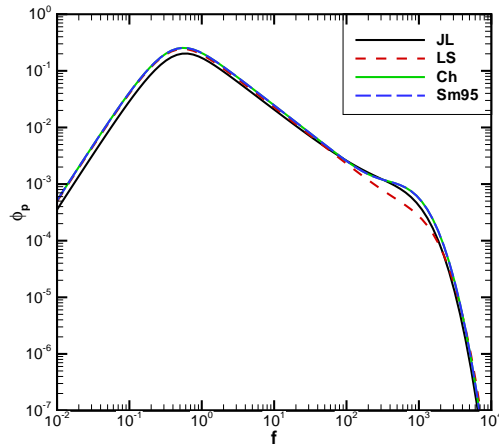


Figure 5. Influence of the turbulence model on the spectrum prediction

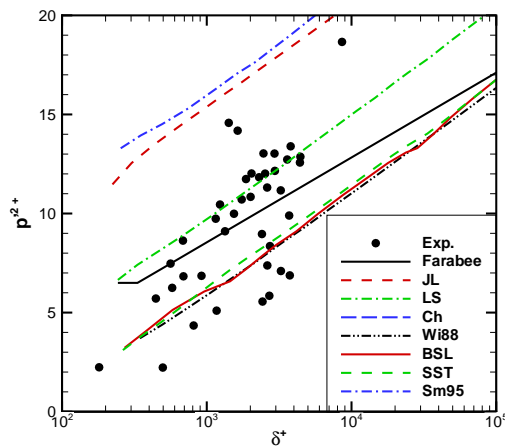


Figure 6. Influence of the turbulence model on the wall pressure variance prediction

i.e. a steeper slope than Farabee and Casarella correlation. An underestimation was expected as the non-linear term in the Poisson equation was neglected while the inactive motions and the outer layer intermittency are not accounted for in a RANS model.

Influence of the turbulence model

Up to now, only the Launder & Sharma (1974) $k - \varepsilon$ model was considered. The method was coupled with a large variety of turbulence models, namely $k - \varepsilon$ models by Jones & Launder (1972) (hereafter denoted JL), Launder & Sharma (1974) (LS) and Chien (1982) (Ch), $k - \omega$ models by Wilcox (1988) (Wi88) and BSL and SST variants by Menter (1994) and $k - L$ model by Smith (1995) (Sm95).

An important issue is the determination of the dissipation rate ε to be used to determine the characteristic wavenumber κ_e . In many turbulence model, the turbulent kinetic energy equation reads

$$\frac{Dk}{Dt} = P_k - \varepsilon - D + \text{div} \left[\left(\nu + \frac{\nu_t}{\sigma_k} \right) \text{grad} k \right] \quad (13)$$

where P_k stands for the turbulent kinetic energy production rate, ε the dissipation rate provided by the length scale determining equation and D is a near wall dissipation term. It has been shown that using $\varepsilon + D$ as the dissipation in the evaluation of the characteristic wavenumber κ_e yields the best behaviour, whatever the turbulence model. Differences are negligible for the Launder and Sharma model while they are larger for the Chien model.

Spectra obtained with the various $k - \varepsilon$ and $k - L$ models are plotted in figure 5 for $R\theta = 10^6$. A fair collapse is obtained for all turbulence models, including $k - \omega$ models (not shown), all models predicting nearly the same k^2 low frequency spectrum and k^{-1} inertial spectrum. The big difference lies in the transition between the inertial and viscous ranges of the spectrum and reflect differences in the wall region treatment among the models. Jones and Launder, Chien and Smith models exhibit a more pronounced and unrealistic bump compared to the Launder and Sharma model while $k - \omega$ models, which underestimate the turbulence in the wall region, exhibit no bump and predict a slightly stronger viscous fall. As the inertial/viscous transition lies in the high frequency regime, its contribution to the integral, i.e. to the pressure variance, is significant. This leads to large differences between the model predictions of the wall pressure variance, as shown in figure 6. The inertial range solution being the same, all models give the same slope but the behaviour in the transition region directly governs the level (A in equation (10)). $k - \omega$ models yield lower levels, in the bottom range of experimental data, Jones and Launder or Smith's models are on the top of the experimental data while Chien model predictions are out of the figure. This shows the strong influence of the near wall region. As most of the assumptions made, such as the use of a simplified velocity spectrum, the symmetry of the two-point correlation or the relation for $\langle v'^2 \rangle$ are poor approximations in this region, further development in the closures in the viscous and buffer region are recommended.

Influence of model coefficients

The influence of the two constant C_{v^2} and C_k introduced to express the Reynolds stress $\langle v'^2 \rangle$ and the characteristic wavenumber κ_e has also been investigated. As can be seen from (1), the Reynolds stress $\langle v'^2 \rangle$ only has a multiplicative rôle while the influence of κ_e is much more complex. Therefore, C_{v^2} acts as a multiplicative constant. Damping it in the buffer and viscous layer is a legitimate and efficient way to suppress the bump in the spectrum at the transition between the inertial and viscous parts. It was shown that C_k strongly affects the predictions. A value of $C_k = 2.0$ nearly collapses the model predictions obtained with the Launder and Sharma model with Farabee and Casarella correlation. The model behaviour can be summarized as

$$\langle p'^2 \rangle^+ = C_{v^2} [A(C_k, \text{Turbulence model}) + B(C_k) \ln \delta^+]$$

ADVERSE PRESSURE GRADIENT BOUNDARY LAYER

Very few detailed experiments are devoted to wall pressure measurements for adverse pressure gradient boundary layers. This lead us to select the experiment by Simpson *et al.* (1987), dealing with an accelerated and then decelerated and separated boundary layer. Only the region up to the

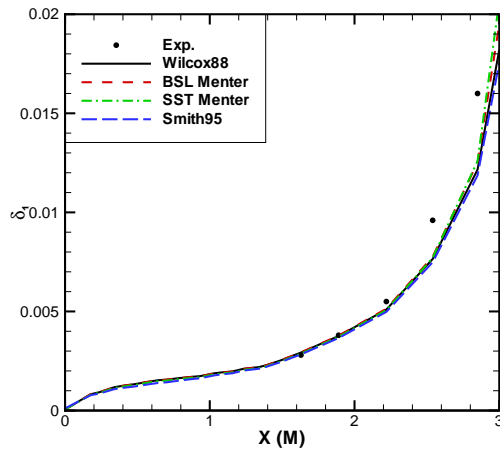


Figure 7. Displacement thickness predictions – Simpson et al. experiment

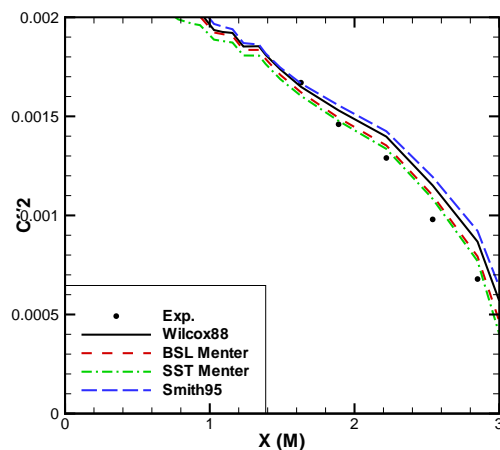


Figure 8. Skin friction coefficient predictions – Simpson et al. experiment

separation point can be computed with the boundary layer approach. Pressure measurements are available only in the decelerated and separated parts. However, it turned out that the boundary layer was not an equilibrium one because of the succession of acceleration and deceleration so that the whole boundary layer development had to be computed. The initial boundary layer thickness had to be tuned to retrieve the correct displacement thickness at the beginning of the deceleration. Only displacement thickness and skin friction coefficient are available at several measurement stations to characterize the boundary layer development. As expected, $k - \varepsilon$ models overestimate the skin friction coefficient and underestimate the displacement thickness. But even $k - \omega$ and $k - L$ models, which are good models to predict adverse pressure gradient flows, fail to reproduce the experiment, as shown in figures 7 and 8. The small differences between BSL and SST models predictions shows that the adverse pressure gradient is not very severe and that the discrepancy, mainly on the displacement thickness, could be blamed upon uncertainties in the external flow distribution.

The pressure variance evolution is plotted in physical

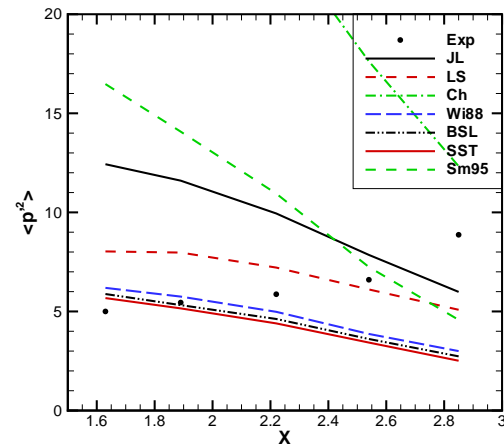


Figure 9. Wall pressure variance evolution – Simpson et al. experiment

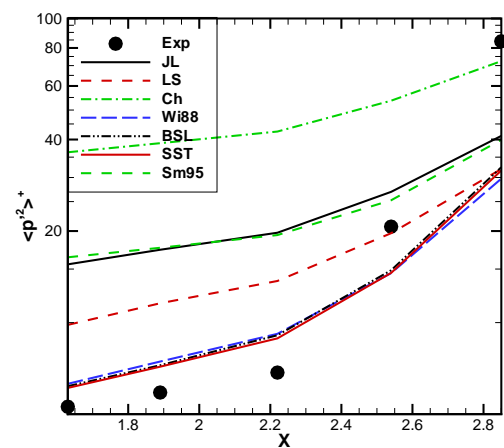


Figure 10. Wall pressure variance (in wall units) evolution – Simpson et al. experiment

units in figure 9 and using wall scaling in figure 10. The differences in the levels for zero pressure gradient boundary layers are retrieved at the initial station, from low levels for $k - \omega$ models to a high level for the Chien model. But all models fail to reproduce the experimental increase of the pressure variance and predict a decrease. Using wall scaling, an increase is observed, thanks to the decrease of the wall shear stress, but the pressure variance remains underestimated.

Various attempts were performed to try to improve the model predictions:

- the EARSM model by Wallin & Johansson (2000) was used to better estimate the Reynolds stress $\langle v'^2 \rangle$,
- the length scale and thus the characteristic wave number κ_e was analytically prescribed, based upon the boundary layer characteristics, instead of using the values deduced from the turbulence model,
- the Taylor hypothesis was replaced by several models linking the convection velocity of the turbulent structures to the external flow velocity.

The first two modifications yield insignificant changes

August 28 - 30, 2013 Poitiers, France

in the predictions of the wall pressure variance while the last one strongly deteriorates the predictions, leading to a stronger decrease of the pressure variance.

The poor predictions can thus be blamed upon various causes:

- A wrong pressure gradient distribution as models under-predicted the displacement thickness evolution,
- An increasing rôle of the non-linear term, which was discarded, for adverse pressure gradient boundary layers as the velocity profile is significantly changed w.r.t. zero pressure gradient boundary layers. The approach could be extended to account for the non-linear term, with some crude assumptions, but this requires significant developments.
- An increasing rôle of the pressure generation by intermittency which cannot be accounted for with standard RANS approaches.

CONCLUSIONS

Following Kraichnan, Lysak proposed a model to evaluate the wall pressure fluctuation spectrum and variance for pipe flows. This approach was extended here to use it as a post-processor of RANS computations. A key improvement is the use of Gauss–Laguerre formula which allows quick and accurate integration.

The model reproduces many nice features of the wall pressure spectrum such as the f^2 behaviour in the low frequency range, the inertial f^{-1} region and the viscous cut-off. The contribution of each part of the boundary layer to the wall pressure spectrum has been identified.

The extension can be performed whatever the turbulence model used. However, because of too crude modelling assumptions, attention has to be paid to the way the model behaves in the transition between the inertial and viscous parts of the spectrum.

Model validation for cases with adverse pressure gradient evidences some problems. Other data are welcome to decide whether there is really a problem in the model. Ways to improve the model to cope with this problem are proposed.

REFERENCES

- Aupoix, B. 2010 Couches limites bidimensionnelles compressibles. Descriptif et mode d'emploi du code CLICET – version 2010. *Tech. Rep.* RT 1/117015 DMAE. ONERA.
- Bradshaw, P., Ferriss, D.H. & Atwell, N.P. 1967 Calculation of boundary-layer development using the turbulent energy equation. *Journal of Fluid Mechanics* **28** (3), 593–616.
- Chien, K.Y. 1982 Predictions of channel and boundary-layer flows with a low-Reynolds-number turbulence model. *AIAA Journal* **20** (1), 33–38.
- Farabee, T.M. & Casarella, M.J. 1991 Spectral features of wall pressure fluctuations beneath turbulent boundary layers. *Physics of Fluids A* **3** (10), 2410–2420.
- Goody, M. 2002 An empirical spectral model of surface-pressure fluctuations that includes Reynolds number effects. In *AIAA/CEAS Aeroacoustics Conference & Exhibit*. The Great Divide Lodge, Breckenridge, Colorado.
- Gravante, S.P., Naguib, A.M., Wark, C.E. & Nagib, H.M. 1998 Characterization of the pressure fluctuations under a fully developed turbulent boundary layer. *AIAA Journal* **36** (10), 1808–1816.
- Hu, Z.W., Morfey, C.L. & Sandham, N.D. 2006 Wall pressure and shear stress spectra from direct simulations of channel flow. *AIAA Journal* **44** (7), 1541–1549.
- Jimnez, J. & Hoyas, S. 2008 Turbulent fluctuations above the buffer layer of wall-bounded flows. *Journal of Fluid Mechanics* **611**, 215–236.
- Jones, W.P. & Launder, B.E. 1972 The prediction of laminarization with a two-equation model of turbulence. *International Journal of Heat and Mass Transfer* **15**, 301–314.
- Launder, B.E. & Sharma, B.I. 1974 Application of energy-dissipation model of turbulence to the calculation of flow near a spinning disc. *Letters in Heat and Mass Transfer* **1**, 131–138.
- Lee, Y.T., Blake, W.K. & Farabee, M. 2005 Prediction of wall pressure spectrum using a RANS calculation. AIAA Paper 2005-802, 43rd Aerospace Science Meeting, Reno, NV.
- Lysak, P.D. 2006 Modeling the wall pressure spectrum in turbulent pipe flow. *Journal of Fluids Engineering* **128**, 216–222.
- Menter, F.R. 1994 Two-equation eddy-viscosity turbulence models for engineering applications. *AIAA Journal* **32** (8), 1598–1605.
- Panton, R.L. & Linebarger, J.H. 1974 Wall pressure spectra calculations for equilibrium boundary layers. *Journal of Fluid Mechanics* **75**, 261–287.
- Simpson, R.L., Ghodbane, M. & McGrath, B.E. 1987 Surface pressure fluctuations in a separating turbulent boundary layer. *Journal of Fluid Mechanics* **177**.
- Skote, M. & Henningson, D.S. 2002 Direct numerical simulation of a separated turbulent boundary layer. *Journal of Fluid Mechanics* **471**, 107–136.
- Smith, B.R. 1995 Prediction of hypersonic shock wave turbulent boundary layer interactions with the $k-l$ two equation turbulence model. AIAA Paper 95-0232 33rd Aerospace Sciences Meeting & Exhibit, Reno, Nevada.
- Spalart, P.R. 1988 Direct simulation of a turbulent boundary layer up to $Re_\theta = 1410$. *Journal of Fluid Mechanics* **187**, 61–98.
- Wallin, S. & Johansson, A.V. 2000 An explicit algebraic Reynolds stress model for incompressible and compressible turbulent flows. *Journal of Fluid Mechanics* **403**, 89–132.
- Wilcox, D.C. 1988 Reassessment of the scale-determining equation for advanced turbulence models. *AIAA Journal* **26** (11), 1299–1310.
- Willmarth, W.W. 1975 Pressure fluctuations beneath turbulent boundary layers. *Annual Review of Fluid Mechanics* **7**, 13–38.